Higher-order resonances in a Stark decelerator

Sebastiaan Y. T. van de Meerakker,[1,2] Nicolas Vanhaecke,[1] Hendrick L. Bethlem,[1,2] and Gerard Meijer[1]

[1]*Fritz-Haber-Institut der Max-Planck-Gesellschaft, Faradayweg 4-6, 14195 Berlin, Germany*
[2]*FOM—Institute for Plasmaphysics Rijnhuizen, Edisonbaan 14, 3439 MN Nieuwegein, The Netherlands*

The motion of polar molecules can be controlled by time-varying inhomogeneous electric fields. In a Stark decelerator, this is exploited to select a fraction of a molecular beam that is accelerated, transported, or decelerated. Phase stability ensures that the selected bunch of molecules is kept together throughout the deceleration process. In this paper an extended description of phase stability in a Stark decelerator is given, including higher-order effects. This analysis predicts a wide variety of resonances that originate from the spatial and temporal periodicity of the electric fields. These resonances are experimentally observed using a beam of OH ($^2\Pi_{3/2}, v=0, J=3/2$) radicals passing through a Stark decelerator.

I. INTRODUCTION

Molecular beams, both continuous and pulsed, are used throughout to produce large densities of molecules in selected quantum states [1]. In these beams, the longitudinal temperature of the molecules is typically 1 K, and the mean velocity of the beam can be varied by adjusting the temperature of the source or by using different seed gases. State selection of a beam of polar molecules can be achieved by actively manipulating the transverse motion of the molecules using electrostatic or magnetic multipole fields as well as with the help of laser radiation [1]. The molecular orientation in space can be actively manipulated as well [2,3]. Molecular beams have therefore been indispensable in a number of research areas like molecular (reactive) scattering studies, high-resolution spectroscopy, and surface science, as well as, for instance, for the production and investigation of transient species.

In recent years our group has developed the so-called Stark deceleration technique, which enables improved control over the longitudinal motion of molecules in a molecular beam. The Stark decelerator for neutral polar molecules is the equivalent of a linear accelerator (LINAC) for charged particles. In the Stark decelerator, the interaction of polar molecules with time-varying electric fields is exploited. A part of a molecular beam can be selected and transferred to any arbitrary velocity, producing bunches of state-selected molecules with a computer-controlled velocity and with longitudinal temperatures as low as a few milliKelvin [4,5]. These experiments are of special interest to the field of cold molecules, as they provide a method to trap relatively high densities of polar molecules at a temperature of a few tens of milliKelvins. In principle, the technique can be applied to any polar molecule that experiences a positive Stark shift in an applied electric field. So far, beams of metastable CO molecules [6], various isotopomers of NH_3 [4], metastable $NH(a\,^1\Delta)$, and ground-state OH radicals [7–9] have been decelerated. In the case of ND_3 and, more recently, OH, the molecules are decelerated to a near standstill and confined in an electrostatic trap [9,10]. Alternatively, after deceleration to about 100 m/s, the molecules can be injected and con-

fined in an electrostatic storage ring [11]. Using a decelerator with a different electrode arrangement, a so-called "alternate gradient" decelerator, molecules with a negative Stark shift can be decelerated as well. This has been demonstrated in proof-of-principle experiments for CO [12] and YbF molecules [13]. A Stark decelerator can also be used to increase the interaction time in a spectroscopic experiment to improve resolution, as is demonstrated in a pump-probe experiment using a decelerated beam of $^{15}ND_3$ molecules [14]. This holds great promise for the use of decelerated molecular beams in experiments aimed at testing fundamental symmetries [15]. In fact, any molecular-beam experiment where the velocity, or velocity distribution, of the molecules is an important parameter can benefit from using a Stark decelerator. In a molecular (reactive) scattering experiment using crossed Stark-decelerated molecular beams, for instance, the scattering process can be studied as a function of the collision energy, probing the potential energy surface with unprecedented detail.

In analogy to the operation of a LINAC [16], the concept of phase stability is essential for the operation of a Stark decelerator [17]. Together with the transverse focusing in the decelerator, phase stability ensures that molecules in a selected (subset of) quantum state(s) can be accelerated, guided, or decelerated without loss, independent of the length of the decelerator; molecules within a certain position and velocity interval are selected and decelerated, keeping the phase-space density of the selected bunch of molecules constant. Phase stability in a Stark decelerator quantitatively governs the dynamics of the selected package, and is fundamental to the understanding of the deceleration process. The same principle of phase stability is essential in the description of schemes for deceleration and bunching of molecules with pulsed traveling optical lattices [18,19].

In recent experiments we have observed sharp and intense resonances in time-of-flight profiles of OH radicals exiting a Stark decelerator, where the available model for phase stability [17] predicts an almost structureless profile. These features strongly suggest that phase stability beyond the current model is present. Numerical trajectory simulations of the experiment accurately reproduce the observations, but such simulations *a priori* yield no understanding of the physical
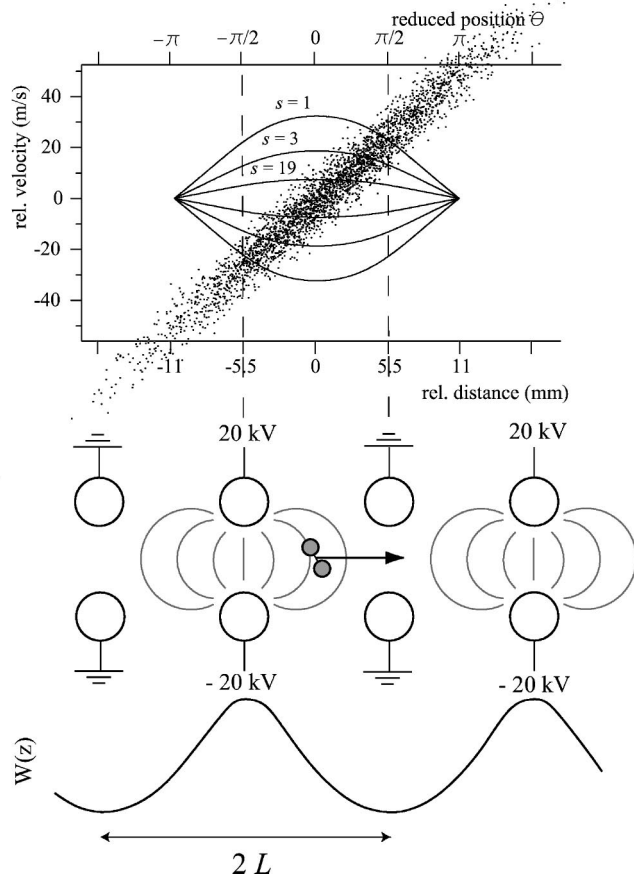
FIG. 1. Scheme of the Stark decelerator, together with the Stark energy of a molecule as a function of position z along the molecular beam axis. Adjacent electric field stages are spaced a distance L =11 mm apart. Each electric field stage consists of two parallel 6-mm-diameter cylindrical rods with a center-to-center distance of 10 mm. A maximum voltage difference of 40 kV is applied to opposing rods in an electric field stage. The longitudinal phase space acceptance of the decelerator for OH($J=3/2$, $M_J\Omega=-9/4$) is given for the resonances $s=1$, 3, and 19 (see text), together with the longitudinal emittance of the OH beam (shaded area).

origin of these features. In this paper, an extended description of phase stability in a Stark decelerator is given, including higher-order terms in the analytical model. Additional phase-stable regions are found that originate from the spatial and temporal periodicity of the electric fields. A comprehensive and intuitive picture of the physical background of these resonances is presented.

II. THEORY

A. Phase stability

The operation principle of a Stark decelerator and a description of phase stability have already been given elsewhere [4,6,17], and this description is only briefly repeated here. The decelerator consists of an array of electric field stages centered a distance L apart, as schematically represented in Fig. 1. Opposing rods are connected to switchable

power supplies with different polarity. All alternating electric field stages are electrically connected to each other. When the odd pairs of electrodes are switched to high voltage, the even pairs are switched to ground, and vice versa. At any given time, the potential energy of a polar molecule as a function of its position has periodicity $2L$. In the extended description of phase stability presented in this paper, it is convenient to describe the motion of a molecule in terms of its reduced position θ, which has periodicity 2π. At a given time t, we define the reduced position $\theta=0$ in between two adjacent pairs of electrodes such that the electrodes at $\theta=\pi/2$ are grounded, as shown in Fig. 1. Switching of the electric field configuration corresponds to a phase shift of θ by π. The reduced position of the molecule at the time the fields are switched is defined as the phase angle ϕ; more precisely, ϕ coincides with θ immediately after the fields have been switched. This definition of ϕ thereby follows the earlier definition made in Refs. [6] and [17].

By definition, a molecule with velocity v_0 is called *synchronous* if its reduced position is always the same at the time the fields are switched, i.e., ϕ_0 remains constant and the kinetic energy of the molecule will change by a constant amount $\Delta K(\phi_0)$ per stage. In the conventional operation of a Stark decelerator, the synchronous molecule achieves this by traveling exactly a distance L in the time ΔT between two successive switch times. This means that the synchronous molecule is always "in phase" with the switching of the decelerator. A molecule that has a slightly different phase ϕ and/or velocity v than the synchronous molecule will experience an automatic correction toward the equilibrium values ϕ_0 and v_0. Molecules within a certain region in phase space, bounded by the so-called separatrix, will undergo stable phase-space oscillations around the synchronous molecule, and a package of molecules is kept together throughout the deceleration process. Molecules outside this bounded region experience the switched potentials as well, but the force on these molecules is expected to be zero on average as they are sometimes accelerated and sometimes decelerated. It is shown in this paper that synchronous molecules and phase stability can be found in this region as well. It is therefore convenient to distinguish between the "switching velocity" of the fields $v_{sw} \equiv L/\Delta T$ and the velocity of the synchronous molecule v_0. We will first derive the equation of motion for phase-stable molecules with $v_0=v_{sw}$, and then extend the description to the cases $v_0 \neq v_{sw}$. In the remainder of this paper, we will refer to the presence of a phase-stable region as a resonance.

B. First-order resonances, $n=1$

In the following, we consider molecules that move along the longitudinal axis of the decelerator. The Stark energy $W(\theta)$ of a polar molecule in a low-field-seeking quantum state is symmetric around the position of a pair of electrodes and can be written as a Fourier series:

$$W(\theta) = \frac{a_0}{2} + \sum_{n=1}^{\infty} a_n \cos[n(\theta + \pi/2)]$$

$$= \frac{a_0}{2} + \sum_{n \text{ odd}} (-1)^{(n+1)/2} a_n \sin n\theta$$

$$+ \sum_{n \text{ even}} (-1)^{n/2} a_n \cos n\theta$$

$$= \frac{a_0}{2} - a_1 \sin\theta - a_2 \cos 2\theta + a_3 \sin 3\theta + \cdots. \quad (1)$$

Since the fields are switched after a time interval ΔT, the force on the molecules is a complicated function of position *and* time. The resulting force can only be integrated numerically, but an intuitive picture can be obtained by introducing the continuously acting *average* force $\bar{F}$ that a molecule experiences between successive switch times. In general, the change in Stark energy of a molecule is small compared to the kinetic energy of the molecule ($\Delta W \ll K$). The change in kinetic energy per stage $\Delta K(\phi_0)$ for a synchronous molecule with phase ϕ_0, and velocity v_0 at a certain switch time is then given by the difference in potential energy at the reduced positions $\theta = \phi_0$ and $\theta = \phi_0 + \pi$:

$$\Delta K(\phi_0) = -\Delta W(\phi_0) = -[W(\phi_0 + \pi) - W(\phi_0)]. \quad (2)$$

The average force $\bar{F}$ that acts on the synchronous molecule is then simply $\bar{F}(\phi_0) = -\Delta W(\phi_0)/L$. This leads to an average force for a synchronous molecule

$$\bar{F}(\phi_0) = -\frac{2a_1}{L} \sin\phi_0, \quad (3)$$

if we take only the terms up to and including $n=1$ in Eq. (1) into account. Under the approximation that a nonsynchronous molecule with phase $\phi = \phi_0 + \Delta\phi$ and a velocity close to v_0 will also experience an average force given by $\bar{F}(\phi_0 + \Delta\phi) = -\Delta W(\phi_0 + \Delta\phi)/L$ between two successive switch times, the equation of motion with respect to the synchronous molecule reads

$$\frac{mL}{\pi} \frac{d^2\Delta\phi}{dt^2} + \frac{2a_1}{L}[\sin(\phi_0 + \Delta\phi) - \sin(\phi_0)], \quad (4)$$

where m is the mass of the molecule [4,6,17]. The outer contour in the phase stability diagram in Fig. 1 is obtained by numerically integrating Eq. (4) for $\phi_0 = 0°$. The area inside this separatrix defines the region in phase space for which nonsynchronous molecules undergo stable oscillations around the synchronous molecule, and gives the longitudinal acceptance of the decelerator. For molecules with a phase and velocity close to those of the synchronous molecule, the oscillation frequency is given by

$$\omega_z/2\pi = \sqrt{\frac{a_1 \cos\phi_0}{2m\pi L^2}}. \quad (5)$$

The size of the separatrix in the velocity direction Δv is proportional to $L\omega_z$. It is noted that operation of the decelerator at $\phi_0 = 0°$ corresponds to transporting (part of) the

beam through the decelerator without deceleration, while acceleration or deceleration of the beam occurs for $-90° < \phi_0 < 0$ and $0 < \phi_0 < 90°$, respectively.

Generally, to investigate the presence of phase-stable regions, we need to calculate ΔW for a molecule in a *given* time interval ΔT. For this, we need to calculate the distance that a molecule travels between successive switch times, which requires knowledge about the velocity of the molecule during the interval ΔT. In the treatment that we use in this paper, we approximate the velocity of a molecule to be constant between two successive switch times. The change in potential energy per stage $\Delta W(\phi_0)$ for a synchronous molecule with phase ϕ_0 and a velocity $v_0 = v_{sw}$ at a certain switch time is then given by $\Delta W(\phi_0) = 2a_1 \sin\phi_0$, if we again take only the terms up to and including $n=1$ in Eq. (1) into account. In the first-order approximation it is assumed that a nonsynchronous molecule with phase $\phi_0 + \Delta\phi$ and velocity v_0 will travel the same distance as the synchronous molecule. This then leads again to the equation of motion given above [Eq. (4)]. In the remainder of this paper, this approach is used to explore the existence of additional stable regions in phase space.

Let us now assume that a synchronous molecule can also exist with a velocity $v_0 \neq v_{sw}$, and introduce the identity $v_0/v_{sw} \equiv s$. Let us again call the phase of the synchronous molecule at a certain switch time ϕ_0. Instead of a distance L this molecule will now travel a distance sL between different switch times, and its reduced position θ on the potential after switching will be

$$\theta = \phi_0 + s\pi + \pi, \quad (6)$$

where the last term π accounts for the switching of the fields. It is readily seen from Eq. (6) that a molecule for which $s = \ell$ (ℓ odd) is indeed synchronous, since its phase on the potential is again ϕ_0 just after the fields are switched. The change in potential energy is given by

$$\Delta W(\phi_0) = 2a_1 \sin\phi_0. \quad (7)$$

In this rather trivial case the synchronous molecule travels an integer number of periods further before the fields are switched than in the case where $v_0 = v_{sw}$. Since the molecule experiences this change in potential energy only after traveling a distance ℓL, the quantity $\Delta W/\ell L$ that is required to derive the equation of motion is a factor ℓ lower compared to $s = \ell = 1$. We can therefore directly use the equation of motion derived earlier if we replace a_1 by a_1/ℓ. This then leads to additional stable regions in phase space around $v_0 = \ell v_{sw}$. The size of the corresponding separatrices in velocity scales as $1/\sqrt{\ell}$ [see Eq. (5)]. The separatrices for $\phi_0 = 0°$ are depicted in Fig. 1 for $s = 3$ and 19 as well.

C. First-order resonances, $n > 1$

So far, only the leading term $a_1 \sin\theta$ in Eq. (1) has been included in the analysis, leading to the series of resonances with $s = \ell$ (ℓ odd). Including higher-order terms will not significantly change the description for molecules whose velocity is close to either one of these resonances. The trajectory of a molecule inside, or close to, a separatrix is dominated by

the term $a_1\sin\theta$, and higher-order terms will only slightly perturb the motion. For velocities further away from these regions, the influence of the a_1 term on the trajectory rapidly decreases, and the terms $a_n\sin n\theta$ with $n>1$ can gain in importance. The even terms in the spatial expansion of the potential energy in Eq. (1) have a maximum at the position of the pair of electrodes that is grounded *and* at the position of the pair that is at high voltage. The contribution of these terms to the potential energy of a molecule is therefore identical before and after switching. The even terms are therefore stationary, and no resonances due to these terms can occur.

The next term in Eq. (1) that needs to be considered is $a_3\sin 3\theta$, which has a periodicity of $2L/3$. A molecule with phase ϕ_0 and velocity $v_0=v_{sw}/3$ travels a distance $L/3$ in the time ΔT between two switch times. This molecule is therefore synchronous with respect to the term $a_3\sin 3\theta$, although it is not synchronous with respect to the leading term $a_1\sin\theta$. If, however, we switch two more times, the reduced position of the molecule will be $\theta=\phi_0+3\pi/3+3\pi=\phi_0$, where the term 3π accounts for the three times switching of the fields. This means that the molecule is synchronous with *both* the $a_1\sin\theta$ and the $a_3\sin 3\theta$ terms every *three* times the fields are switched. This, however, does not automatically imply that a phase-stable region exists around this synchronous molecule. As before, we need to show that a nonsynchronous molecule with position $\phi=\phi_0+\Delta\phi$ and/or velocity $v=v_0+\Delta v$ experiences a correction towards the equilibrium values ϕ_0 and v_0. Analogous to Eq. (2) we need to calculate the energy $\Delta W(\phi)$ that a (non)synchronous molecule loses after three times switching. In general, a molecule with velocity sv_{sw} travels a distance $s\pi$ between successive switch times, and it can be shown that $\Delta W(\phi)$ after Q times switching can be written as

$$\Delta W(\phi) = \sum_{n \text{ odd}} (-1)^{(n+1)/2}\left(\sum_{q=0}^{Q}\{-2a_n\sin[n\phi+qn(s+1)\pi]\}\right.$$
$$+ a_n\sin(n\phi) + a_n\sin[n\phi+Qn(s+1)\pi]\bigg)$$
$$+ \sum_{n \text{ even}} (-1)^{n/2}\{a_n\cos[n\phi+Qn(s+1)\pi]$$
$$- a_n\cos(n\phi)\} \tag{8}$$

if we take into account all Fourier terms of Eq. (1). For the situation discussed above we have $s=1/3$, leading to an energy loss for the synchronous molecule after three times switching ($Q=3$) of

$$\Delta W(\phi_0) = -3 \times 2a_3\sin 3\phi_0 = 3 \times 2a_3\sin 3\left(\phi_0+\frac{\pi}{3}\right) \tag{9}$$

if we take terms up to and including $n=3$ in Eq. (1) into account. It is seen that the energy loss of the molecules due to the dominant term $a_1\sin\theta$ in Eq. (1) is zero after *three* times switching, while the energy loss resulting from the term $a_3\sin 3\theta$ adds up *every* time we switch. The situation can thus conveniently be described as if the potential energy of the molecule in the decelerator is only given by $W(\theta)$

$=a_3\sin 3\theta$. Hence, the equation of motion of molecules with respect to the synchronous molecule is given by Eq. (4) when a_1 is substituted by a_3, L by $L/3$, and ϕ by $3(\phi+\pi/3)$, respectively. The opposite sign in front of the term $a_3\sin 3\theta$ with respect to the term $a_1\sin\theta$ in Eq. (1) is equivalent to a phase shift of $\pi/3$. Inclusion of the term $n=3$ in the analysis leads to additional stable regions in phase space around the velocity $v_0=v_{sw}/3$. As in the case $n=1$ discussed in the previous section, a series of resonances is present around the velocities $v_0=\ell v_{sw}/3$ (ℓ odd).

Including even higher-order terms of Eq. (1) in the analysis, and with the help of Eq. (8), in general resonances occur at $s=\ell/n$ (both ℓ and n odd). For a given value of n, the force on a synchronous molecule due to the more dominant terms $<n$ cancels after n times switching, whereas the remaining leading term $a_n\sin n\theta$ results in a force $(2a_n/\ell L)\sin n\phi_0$ every time the fields are switched. The corresponding separatrices have periodicity $2L/n$, and the longitudinal oscillation frequency is given by

$$\omega_z/2\pi = \sqrt{\frac{a_n\cos n\phi_0}{2m\pi sL^2}}. \tag{10}$$

Since these resonances at velocities $v_0=(\ell/n)v_{sw}$ can already be derived in the first-order approximation for the motion of the molecules through the Stark decelerator, we refer to these as first-order resonances.

An interpretation of the resonances $s=\ell/n$ can be obtained by representing both the spatial and the temporal dependence of the potential as a Fourier series. It was shown that the resulting force $F(\phi,t)$ that acts on the molecules can be written as

$$F(\phi,t) = \sum_{n \text{ even}}^{\infty} \frac{\pi n}{L}a_n\cos(n\phi) - \sum_{\ell \text{ odd}}^{\infty}\sum_{n \text{ odd}}^{\infty} \frac{2n}{\ell L}a_n\sin(n\phi-\ell\omega t), \tag{11}$$

where $\omega=2\pi/\Delta T$ [20]. It is seen that the force is composed of a sum over stationary waves (n even) and propagating partial waves $\sin(n\phi-\ell\omega t)$ that move with phase velocity $v_\phi=(\ell/n)v_{sw}$. Resonances occur if the velocity v_0 of a molecule corresponds to the phase velocity v_ϕ of a propagating partial wave. Molecules with velocities that are close to this value interact strongly with the corresponding partial wave, while the more dominant partial waves have on average no effect on the motion; a synchronous molecule with $s=\ell/n$ is trapped at the center of the traveling potential well produced by the corresponding propagating partial wave ℓ, n.

D. Numerical simulations

In this section, numerical simulations of the trajectories of molecules through a Stark decelerator are discussed. The stable regions in phase space can be visualized by calculating the average velocity of a molecule during its trajectory through the decelerator. If a molecule is within a phase-stable region, it will rotate in phase space around the corresponding synchronous molecule, and hence the average velocity of this molecule will be identical to the average
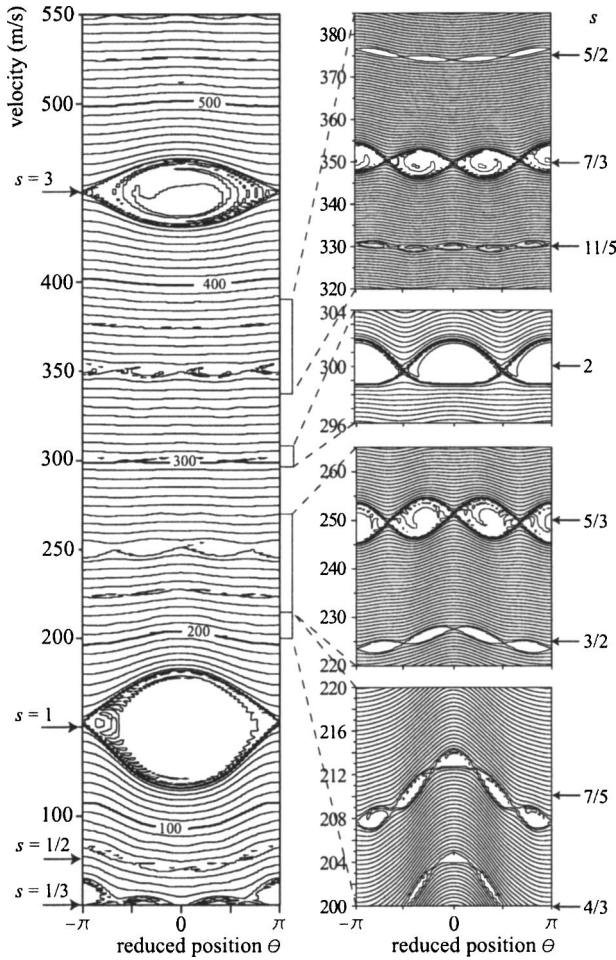
FIG. 2. Contour plot of the average velocity of OH(J =3/2, $M\Omega=-9/4$) radicals as a function of their initial position and velocity, that results from a one-dimensional numerical simulation of their trajectories through a 300-stage decelerator. The decelerator is operated at a phase angle $\phi_0=0°$ and a "switching velocity" $v_{sw}=150$ m/s. Resonances appear as regions in phase space where all the molecules have the same average velocity. The structure inside the separatrices is a result of the finite number of stages used in the simulation.

velocity of the synchronous molecule [20]. Resonances therefore appear as regions in phase space where all the molecules have the same average velocity. The trajectories of molecules in a Stark decelerator are calculated by numerically integrating the equation of motion of the molecules. From a calculation of the electric field distribution in an electric field stage in combination with the (quantum state specific) Stark effect of the molecule of interest, the coefficients of the spatial Fourier expansion as given in Eq. (1) are determined. For OH radicals in the $J=3/2$, $M\Omega=-9/4$ component, the relevant odd coefficients are $a_1=0.618$ cm^{-1}, $a_3=0.044$ cm^{-1}, and $a_5=0.0037$ cm^{-1} for the geometry and voltage settings of the decelerator used in the present experiments (see below).

Figure 2 depicts a contour plot of the average velocity of OH($J=3/2$,$M\Omega=-9/4$) radicals as a function of their initial position and velocity, which results from a one-dimensional numerical simulation of their trajectories through a 300-stage

decelerator. The decelerator is operated at a phase angle ϕ_0 =0° and at a constant "switching velocity" $v_{sw}=150$ m/s. The switching of the high voltage in the decelerator is assumed to be instantaneous. The initial positions and velocities of the molecules are deterministically distributed on a grid that covers two full stages in position (from $-\pi$ to $+\pi$ in reduced position θ) and that ranges from 50 to 550 m/s in velocity. The first-order resonances $s=1$ at velocity v_0 =v_{sw}(150 m/s), and $s=3(v_0=3v_{sw}=450$ m/s) are clearly identified. The structure inside the separatrices is a result of the finite number of stages used in the simulation. The size and shape of the separatrices are in quantitative agreement with the model described in Secs. II B and II C. In particular, the compression of the separatrix along the velocity direction for $s=3$ by $\sqrt{3}$ with respect to $s=1$, as predicted by the model, is observed. The slight asymmetry of the separatrix for $s=1$ is the result of higher-order effects that are neglected thus far in the model.

In the panel on the right-hand side of Fig. 2, four selected phase-space regions are shown on an expanded vertical scale; note that the vertical scale for each of the regions is different. The resonances with $s=5/3$ at $v_0=250$ m/s and $s=7/3$ at $v_0=350$ m/s that belong to the series of first-order resonances with $n=3$ are clearly visible and, as predicted by the model, have periodicity $2\pi/3$. The opposite sign in front of the term $a_3\sin 3\theta$ with respect to the term $a_1\sin \theta$ in Eq. (1) results in a phase shift of $\pi/3$, and the centers of the separatrices are found at the reduced positions $\theta=-\pi$, $-\pi/3$, $\pi/3$, and π. The resonances with $s=7/5$ and $11/5$ that belong to the series $n=5$ can be also clearly identified, even though the coefficient a_5 is about an order of magnitude smaller than a_3. The centers of the corresponding separatrices are not phase shifted relative to the resonance $s=1$ and are found at the positions $\theta=-4\pi/5$, $-2\pi/5$, 0, $2\pi/5$, and $4\pi/5$.

In general, the size, shape, and position of the phase stable regions in Fig. 2 that belong to the first-order resonances $s=\ell/n$ (ℓ and n odd) are quantitatively reproduced by the model. The distortions in the shape of the separatrices for, for instance, the resonances with $s=5/3$ and $7/5$ are due to the dominant term $a_1\sin \theta$ in Eq. (1). The influence of this term on the motion of the molecules is *only* zero after an appropriate number of switch times, but for intermediate times, the trajectory of the molecules is predominantly determined by this term. This is most apparent for the resonance $s=7/5$ as this resonance is very close to the resonance $s=1$. The curve that connects the centers of the five separatrices is to be interpreted as the influence of the (dominant) term $a_1\sin \theta$ on the velocity of the synchronous molecule. Only after five switch times does this influence cancel, and the synchronous molecule has not lost, or gained, kinetic energy due to the term $a_1\sin \theta$.

Apart from the resonances $s=\ell/n$ (ℓ and n odd) discussed in Secs. II B and II C, additional resonances are observed. These resonances occur at $s=1/2(75$ m/s), $3/2(225$ m/s), and $5/2(375$ m/s) with a periodicity $2\pi/4$ and at s =2(300 m/s) with a periodicity $2\pi/2$. Applying Eq. (8) to these cases gives $\Delta W(\phi)=0$ for all ϕ. Similarly, these resonances do not correspond to any propagating partial wave in

the force $F(\phi,t)$ [Eq. (11)]. Clearly, these resonances cannot be explained with the model used thus far, suggesting that more subtle effects in the dynamics of the molecules inside the Stark decelerator need to be taken into account. This is the topic of the next section.

E. Second-order resonances

So far, to calculate the change in potential energy ΔW in the time ΔT between two switch times, the approximation has been made that the velocity of a (non)synchronous molecule remains constant. With this approximation, a nonsynchronous molecule with phase $\phi_0+\Delta\phi$ and a synchronous molecule, both with velocity v_0 at a certain switch time, will travel the same distance $v_0 L/v_{sw}$ in the time ΔT. The change in potential energy $\Delta W(\phi)$ for (non)synchronous molecules after Q times switching is then given by Eq. (8), and leads to the resonances $s=\ell/n$ (ℓ and n odd).

A more accurate description of the motion of molecules in a Stark decelerator is obtained when the approximation that the velocity of a molecule during the time interval ΔT is constant is refined. In the following we will discriminate between the *average* velocity $\langle v \rangle$ of a molecule during ΔT and the *instantaneous* velocity v of a molecule at the time the fields are switched. Again we compare a nonsynchronous molecule with phase $\phi_0+\Delta\phi$ and a synchronous molecule with phase ϕ_0, both with the same instantaneous velocity v_0 at the time the fields are switched. The nonsynchronous molecule traverses a different part of the potential and will have a *different* average velocity in the time ΔT than the synchronous molecule. In contrast to the approximation used before, the distances that a nonsynchronous and a synchronous molecule travel in the time ΔT will now be different, and higher-order terms appear in the expression for $\Delta W(\phi)$ in Eq. (8). These higher-order terms can lead to $\Delta W(\phi) \neq 0$ for those cases where Eq. (8) leads to $\Delta W(\phi)=0$, and it is shown in the remainder of this section that these terms can explain the additional resonances discussed in Sec. II D.

1. The series $s=2, 4, 6, \ldots$

Referring back to Fig. 2, the resonance at $s=2$ with periodicity π suggests that the corresponding synchronous molecule with phase ϕ_0 at a certain switch time k has an average velocity $\langle v_0 \rangle = 2v_{sw}$ between switch times k and $k+2$, and that its change in kinetic energy is proportional to $\sin(2\phi_0)$. However, neither the instantaneous velocity v_0 of the synchronous molecule at the switch time k, nor the average velocity between the switch times k and $k+1$, nor that between the switch times $k+1$ and $k+2$ is known. It is therefore convenient to use the superscript k in the expressions for the phase ϕ, for the potential energy W, for the kinetic energy K, and for the velocity v of a molecule at the switch time k.

Let us consider a molecule that at a certain switch time k has an *instantaneous* velocity v_0^k and a phase ϕ_0^k. For this molecule to be synchronous, its average velocity between switch times k and $k+2$ has to obey $\langle v_0 \rangle^{k,k+2}=2v_{sw}$. As before, to study the possible existence of a resonance, we need to calculate the difference in potential energy $\Delta W^{k,k+2}$ of this molecule between switch times k and $k+2$:

$$\Delta W^{k,k+2} = \Delta W^{k,k+1} + \Delta W^{k+1,k+2}. \tag{12}$$

When we take only terms up to and including $n=1$ of Eq. (1) into account, the change in potential energy $\Delta W^{k,k+1}$ of the synchronous molecule between switch times k and $k+1$ is given by

$$\begin{aligned}\Delta W^{k,k+1} &= W(\phi_0^k + \Delta\theta^{k,k+1}) - W(\phi_0^k) \\ &= -a_1\sin(\phi_0^k + \Delta\theta^{k,k+1}) + a_1\sin\phi_0^k \\ &\approx -a_1(\Delta\theta^{k,k+1} - 2\pi)\cos\phi_0^k. \end{aligned} \tag{13}$$

In this expression $\Delta\theta^{k,k+1}$ is the distance the molecule travels between switch times k and $k+1$. The approximation in the last line of Eq. (13) is made because $\Delta\theta^{k,k+1}$ is close to 2π in this case (see below). The distance $\Delta\theta^{k,k+1}$ follows from the *average* velocity of the molecule between the switch times k and $k+1$, which will be close, but not necessarily equal, to $2v_{sw}$. The average velocity $\langle v \rangle^{k,k+1}$ of the synchronous molecule follows from the conservation of energy:

$$K(v_0^k) + W(\phi_0^k) = \frac{1}{2}m\langle v^2 \rangle^{k,k+1} + \langle W \rangle^{k,k+1} \tag{14}$$

in the approximation that $(\langle v \rangle^{k,k+1})^2$ equals $\langle v^2 \rangle^{k,k+1}$. It can be shown that in this approximation $\langle W \rangle^{k,k+1}$ is equal to zero for the series $s=2, 4, 6, \ldots$ (proof available upon request), resulting in

$$\begin{aligned}\langle v \rangle^{k,k+1} &\approx \sqrt{\frac{2}{m}[K(v_0^k) + W(\phi_0^k)]} = v_0^k \sqrt{1 + \frac{W(\phi_0^k)}{K(v_0^k)}} \\ &\approx v_0^k\left(1 - \frac{a_1\sin\phi_0^k}{m(v_0^k)^2}\right). \end{aligned} \tag{15}$$

The distance $\Delta\theta^{k,k+1}$ that the molecule travels between switch times k and $k+1$ is then given by

$$\Delta\theta^{k,k+1} = \pi\left(\frac{\langle v \rangle^{k,k+1}}{v_{sw}}\right) \approx 2\pi\frac{v_0^k}{2v_{sw}}\left(1 - \frac{a_1\sin\phi_0^k}{m(v_0^k)^2}\right). \tag{16}$$

To calculate the change of potential energy $\Delta W^{k+1,k+2}$ of the synchronous molecule between switch times $k+1$ and $k+2$, the analysis given above is repeated for a molecule at reduced position θ^{k+1} and velocity v_0^{k+1} at switch time $k+1$. The reduced position θ^{k+1} of the molecule on the potential just after switch time $k+1$ is given by

$$\theta^{k+1} = \phi_0^k + \Delta\theta^{k,k+1} + \pi, \tag{17}$$

where the term π accounts for the switching of the fields. Therefore,

$$\begin{aligned}\Delta W^{k+1,k+2} &= W(\theta^{k+1} + \Delta\theta^{k+1,k+2}) - W(\theta^{k+1}) \\ &\approx -a_1(\Delta\theta^{k+1,k+2} - 2\pi)\cos\theta^{k+1} \\ &\approx a_1(\Delta\theta^{k+1,k+2} - 2\pi)\cos\phi_0^k, \end{aligned} \tag{18}$$

where in the last step the approximation has been used that $\Delta\theta^{k,k+1}$ is close to 2π. The distance $\Delta\theta^{k+1,k+2}$ follows from the *average* velocity of the molecule between the switch times $k+1$ and $k+2$. The average velocity $\langle v \rangle^{k+1,k+2}$ of the

synchronous molecule follows from the conservation of energy:

$$K(v_0^{k+1}) + W(\theta^{k+1}) = \frac{1}{2}m\langle v^2 \rangle^{k+1,k+2} + \langle W \rangle^{k+1,k+2}. \quad (19)$$

Since $\langle W^{k+1,k+2} \rangle$ is again zero in this case, the average velocity $\langle v \rangle^{k+1,k+2}$ of the molecule between switch times $k+1$ and $k+2$ is approximated by

$$\langle v \rangle^{k+1,k+2} \approx v_0^{k+1}\left(1 - \frac{a_1 \sin \theta^{k+1}}{m(v_0^{k+1})^2}\right). \quad (20)$$

It is convenient to express v_0^{k+1} in terms of v_0^k, which follows from the conservation of energy and Eq. (13) as

$$v_0^{k+1} = \sqrt{(v_0^k)^2 + \frac{2a_1}{m}(\Delta\theta^{k,k+1} - 2\pi)\cos \phi_0^k}. \quad (21)$$

The synchronous molecule then travels a distance $\Delta\theta^{k+1,k+2}$ between switch times $k+1$ and $k+2$, given by

$$\Delta\theta^{k+1,k+2} = \pi\left(\frac{\langle v \rangle^{k+1,k+2}}{v_{\text{sw}}}\right) \approx 2\pi\frac{v_0^k}{2v_{\text{sw}}}\left(1 + \frac{a_1 \sin \phi_0^k}{m(v_0^k)^2}\right). \quad (22)$$

The reduced position θ^{k+2} of the synchronous molecule at switch time $k+2$, just after switching, is

$$\theta^{k+2} = \phi_0^k + (\Delta\theta^{k,k+1} + \pi) + (\Delta\theta^{k+1,k+2} + \pi)$$

$$\approx \phi_0^k + 4\pi\frac{v_0^k}{2v_{\text{sw}}} + 2\pi. \quad (23)$$

As mentioned before, the average velocity between switch times k and $k+2$ has to be $2v_{\text{sw}}$ for the molecule to be synchronous. With respect to the initial phase ϕ_0^k, its reduced position θ^{k+2} just after switch time $k+2$ therefore has to be $\phi_0^k + 4\pi + 2\pi$, where the term 2π accounts for the two times switching. From Eq. (23) it then follows that its instantaneous velocity v_0^k at switch time k needs to be *identical* to its average velocity $2v_{\text{sw}}$ between switch times k and $k+2$: $v_0^k = 2v_{\text{sw}}$. It is noted that this is coincidentally the case for the special series $s = 2, 4, 6, \ldots$ discussed here, but that this is not generally true for the resonances of second order (see below).

Finally, the total change in potential energy of the molecule between switch times k and $k+2$ can now be calculated:

$$\Delta W(\phi_0^k) = \Delta W^{k,k+1} + \Delta W^{k+1,k+2}$$

$$\approx a_1(\Delta\theta^{k+1,k+2} - \Delta\theta^{k,k+1})\cos \phi_0^k$$

$$\approx \frac{4\pi a_1^2}{m(2v_{\text{sw}})^2}\sin \phi_0^k \cos \phi_0^k$$

$$= \frac{2\pi a_1^2}{m(2v_{\text{sw}})^2}\sin 2\phi_0^k. \quad (24)$$

The second-order terms in the derivation thus result in an expression for $\Delta W(\phi_0)$ that is similar to the expression found before for the first-order resonances $s = \ell/n$. The derivation

given above is also valid for a nonsynchronous molecule with phase $\phi^k = \phi_0^k + (\Delta\phi)^k$ and with velocity v_0^k at switch time k if the synchronous phase ϕ_0 in the expressions above is replaced by $\phi_0^k + (\Delta\phi)^k$. A nonsynchronous molecule will therefore lose a kinetic energy $-\Delta W(\phi_0^k + (\Delta\phi)^k)$. For the resonances in Fig. 2, the decelerator is operated at $\phi_0 = 0°$, and the equation of motion for nonsynchronous molecules with respect to the synchronous molecule in this case is again given by Eq. (4) with the appropriate substitutions. The size of the separatrix in the velocity direction depends now not only on the appropriate coefficient of the spatial Fourier expansion of the field, but has an additional factor that is proportional to the ratio of the potential energy to the kinetic energy. In contrast to the first-order resonances the size of the phase-stable regions for these so-called second-order resonances rapidly decreases with higher "switching velocities" of the decelerator. The size of the separatrices belonging to the resonance $s = 2$ in Fig. 2 is quantitatively reproduced by the model. The derivation given in this section can be further generalized to describe additional resonances for $s = 2\ell$ (ℓ integer) as well.

2. The series $s = 1/2, 3/2, 5/2, \ldots$

Referring back to Fig. 2, the observed resonances at $s = \ell/2$ (ℓ odd) with periodicity $2\pi/4$ suggest that the change in potential energy of the corresponding synchronous molecule, after four times switching, is proportional to $\sin(4\phi_0)$. To explain these resonances higher-order terms in the Fourier expansion of Eq. (1) need to be included in the analysis. This series of resonances can be described when the terms $a_1 \sin \theta$ and $a_3 \sin 3\theta$ are taken into account; this derivation is not explicitly given here, but is available upon request. Again we consider a molecule with phase ϕ_0^k and velocity v_0^k at a certain switch time k, and we calculate the energy difference $\Delta W_0^{k,k+4}$ between switch times k and $k+4$. For the resonance $s = 1/2$ the instantaneous velocity v_0^k at switch time k has to be

$$v_0^k = \frac{v_{\text{sw}}}{2}\left[1 - \frac{a_1}{mv_{\text{sw}}^2}\cos \phi_0^k - \frac{a_3}{mv_{\text{sw}}^2}\cos 3\phi_0^k\right] \quad (25)$$

in order for the synchronous molecule to have an average velocity of $\langle v_{\text{synchr}} \rangle = v_{\text{sw}}/2$ between switch times k and $k+4$. The kinetic energy that the synchronous molecule loses after four times switching is

$$\Delta W(\phi_0^k) = \frac{2\pi a_1 a_3}{m(v_{\text{sw}}/2)^2}\left(4 - \frac{16}{3\pi}\right)\sin 4(\phi_0^k - \pi/4) \quad (26)$$

neglecting terms of higher order in (W/K). This expression has again the familiar form that leads to phase stability. The resulting separatrices have periodicity $2\pi/4$, and are phase shifted by $\pi/4$ with respect to $\phi_0^k = 0$ since the product $a_1 a_3 > 0$. Note that no terms proportional to a_1^2 or a_3^2 appear in the expression for $\Delta W(\phi_0^k)$, and that it is the cross term proportional to $a_1 a_3$ which gives rise to the resonance. A nonsynchronous molecule with initial phase $\phi^k = \phi_0^k + (\Delta\phi)^k$ and with initial velocity v^k that obeys Eq. (25) loses a kinetic energy $-\Delta W[\phi_0^k + (\Delta\phi)^k]$, and will oscillate in phase space

around the equilibrium values ϕ_0 and v_0 of the synchronous molecule.

The velocity of the synchronous molecule at every switch time between k and $k+4$ is not constant, as is evident from the curved line that connects the four separatrices in Fig. 2. This curve $v_0(\theta)$ is given by Eq. (25), when ϕ_0^k is replaced by θ, and represents the influence of the leading term $a_1\sin\theta$ on the motion of the molecules, which only cancels after four times switching. It is clear that the entire series of second-order resonances with $s=\ell/2$ (ℓ odd) can be explained by this model. The phase-stable regions obtained from the simulation for $s=3/2$ and $5/2$ (see Fig. 2) can be quantitatively reproduced.

3. Other resonances

In Fig. 2 a resonance is also seen at $s=4/3(v=200$ m/s$)$. Although the derivation has not been explicitly made for this, it is believed that, in analogy with the derivation for the series $s=2\ell$ (ℓ integer), the term $a_3\sin 3\theta$ gives rise to resonances at $s=2\ell/3$ (ℓ integer). The corresponding kinetic energy loss for the synchronous molecule is proportional to $(a_3^2/mv_{sw}^2)\sin 6\phi_0^k$, and the separatrices have periodicity $2\pi/6$. This interpretation is supported by numerical simulations. In fact, the simulations indicate that many more resonances exist as well. For example, the resonances $s=1/5$ and $1/7$ already appear even if the terms $a_5\sin 5\theta$ and $a_7\sin 7\theta$ in the spatial Fourier expansion of the potential [Eq. (1)] are set to zero in the simulations, although the size of the separatrices is then rather small. Although speculative, these resonances are believed to originate from the neglected terms that are proportional to $(W/K)^2$, and $\Delta W(\phi_0^k)$ for a synchronous molecule takes the form

$$\Delta W(\phi_0^k) \propto \frac{a_1^2 a_3}{m^2 v_{sw}^4}\sin 5\phi_0^k \qquad (27)$$

and

$$\Delta W(\phi_0^k) \propto \frac{a_1 a_3^2}{m^2 v_{sw}^4}\sin 7\phi_0^k \qquad (28)$$

for the resonances $s=1/5$ and $1/7$, after switching five and seven times, respectively. Including the terms $a_5\sin 5\theta$, etc., in the analysis and/or taking even higher-order terms in W/K into account will lead to additional resonances, but this is beyond the scope of this paper.

F. Summary

In the previous sections the longitudinal motion of molecules through a Stark decelerator is described using models with different levels of approximation. In the first-order approximation, the influence of the potential energy on the motion of the molecules in the time interval ΔT between successive switch times is neglected, and the molecule is assumed to have a constant velocity during this time interval. With this approximation, the resonances $s=\ell/n$ (both ℓ and n odd) can be explained. The change in potential energy of a synchronous molecule after n times switching can generally be expressed as
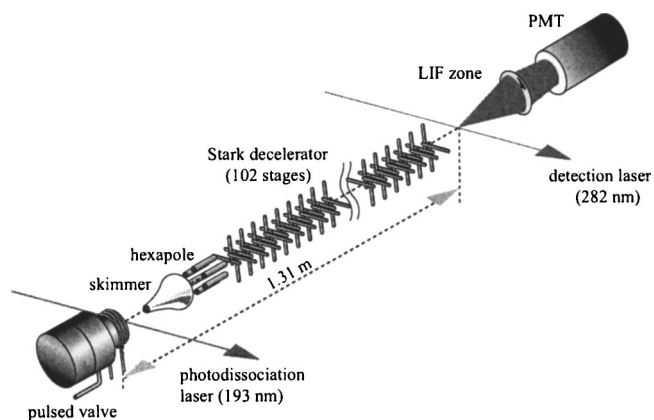

FIG. 3. Scheme of the experimental setup. A pulsed beam of OH with a mean velocity of 450 m/s is produced via ArF-laser photo-dissociation of HNO_3 seeded in Kr. The molecular beam passes through a skimmer, hexapole, and Stark decelerator into the detection region. State-selective LIF detection is used to measure the arrival time distribution of the OH($J=3/2$) radicals that exit the decelerator.

$$\Delta W(\phi_0) = -(-1)^{(n+1)/2}2na_n\sin n\phi_0. \qquad (29)$$

The corresponding separatrices have periodicity $2\pi/n$, and their size does not depend on v_{sw}. These resonances are referred to as first-order resonances.

In the second-order approximation, the influence of the potential energy on the motion of the molecules in the time interval ΔT is taken into account. With this approximation, additional series of resonances are found; the derivation for the cases $s=2\ell$ (ℓ integer) and $s=\ell/2$ (ℓ odd) has been made. The expressions for $\Delta W(\phi_0)$ for the synchronous molecules are proportional to W/K. Even higher-order resonances exist as well, but a discussion of these is beyond the scope of this paper.

III. EXPERIMENT

A. Experimental setup

The experiments described in this paper are performed in a new generation molecular beam deceleration machine which is shown schematically in Fig. 3. Recently, this machine has been used to decelerate and electrostatically trap OH radicals [9]. The experiments reported in this paper are performed on OH radicals as well. For this, a pulsed beam of OH radicals is produced by photodissociation of HNO_3, co-expanded with Kr from a pulsed solenoid valve. The 193 nm pulsed UV radiation from a compact excimer laser is focussed onto, but near the exit of, a quartz capillary that is mounted on the nozzle orifice [21]. The OH radicals are thus prepared at a well-defined position and time, which considerably simplifies the interpretation of the observed time-of-flight (TOF) profiles. The mean velocity of the beam is around 450 m/s with a velocity spread [full width at half maximum (FWHM)] of about 15%. After the supersonic expansion, most of the OH radicals in the beam reside in the lowest rotational ($J=3/2$) level in the vibrational and electronic ground state $X\,^2\Pi_{3/2},v''=0$. This level has a Λ-doublet

splitting of 0.055 cm^{-1}. The low-field-seeking upper Λ-doublet component of f parity [22] is split into an $M_J\Omega$ $=-3/4$ and an $M_J\Omega=-9/4$ component when an electric field is applied. The $M_J\Omega=-9/4$ component has a three times larger Stark shift than the $M_J\Omega=-3/4$ component. The molecular beam passes through a 2-mm-diameter skimmer, and enters a second vacuum chamber where the OH molecules are transversely focused into the Stark decelerator using a short pulsed hexapole. The more than 1-m-long Stark decelerator consists of an array of 102 equidistant electric field stages, with a center-to-center distance L of adjacent stages of 11 mm. Each stage consists of two parallel 6-mm-diameter polished hardened steel rods that are symmetrically located around the beam axis with a center-to-center distance of 10 mm. All alternating stages are rotated by 90° with respect to each other, providing a 4×4 mm^2 transverse spatial acceptance area. The decelerator is operated using a voltage difference of 40 kV between opposing electrodes in a field stage, creating a maximum electric field strength on the molecular beam axis of about 90 kV/cm. The individual electrodes of alternating stages are electrically connected to an oil-cooled high-voltage switch (Behlke Elektronik HTS 651-03-GSM), requiring a total number of four independent switches for the decelerator. Every switch is connected to a 300 nF capacitor bank that delivers the high voltage during a time sequence, limiting the voltage drop during a burst to only 3%. The OH radicals are state selectively detected 109 mm downstream from the decelerator (1307 mm from the nozzle) using a laser-induced fluorescence (LIF) detection scheme. The 282 nm radiation of a pulsed dye laser crosses the molecular beam at right angles and induces the $Q_1(1)$ transition of the $A\,^2\Sigma^+,v'=1\leftarrow X\,^2\Pi_{3/2},v''=0$ band. Typically, 1.5 mJ of radiation in a 0.1 cm^{-1} spectral bandwidth in a 5 ns pulse is used, sufficient to saturate the transition. The off-resonant fluorescence on the $A\,^2\Sigma^+,v'=1\rightarrow X\,^2\Pi_{3/2},v''$ $=1$ band around 313 nm is imaged onto a photomultiplier tube (PMT) using a lens system. OH radicals in both low-field-seeking $M_J\Omega$ components of the $J=3/2$ level contribute to the LIF signal. Stray light from the laser is reduced by passing the laser beam through light baffles and is further suppressed by optical filtering in front of the PMT.

B. First-order resonances

In the experiments described in this paper, the decelerator is operated with equal time intervals in a single time sequence, corresponding to transporting (part) of the beam through the decelerator without deceleration, i.e., the decelerator is operated at a phase angle of 0°. The advantage of that is that the interpretation of time-of-flight profiles of the molecules exiting the decelerator is straightforward. A certain arrival time (almost) directly corresponds to a certain velocity of the molecule. The arrival time distribution (TOF profile) of the OH($J=3/2$) radicals is recorded by scanning the time delay between the detection laser and the dissociation laser. The first pair of electrodes of the decelerator is switched to high voltage when the most intense part of the beam is at position $\theta=0$ in the first electric field stage, thereby coupling in the molecular beam in the center of the
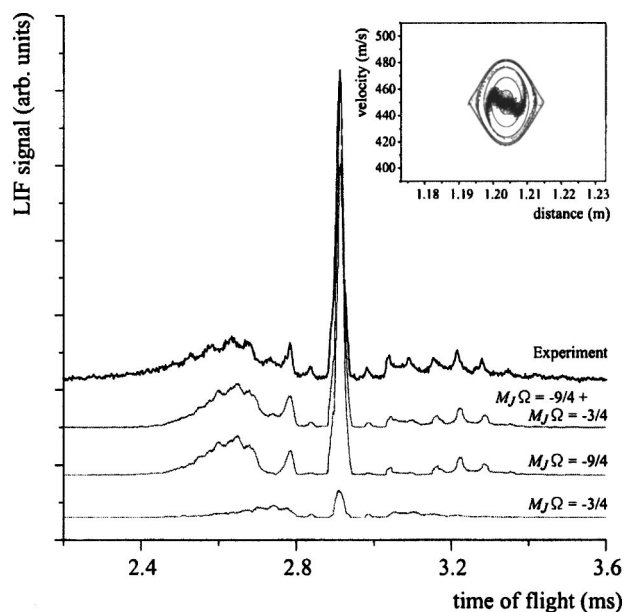

FIG. 4. Observed TOF profile when the decelerator is operated at $v_{sw}=450.0$ m/s and phase angle $\phi_0=0°$. The TOF profile that is obtained from a three-dimensional trajectory simulation of the experiment is shown underneath the experimental profile. The individual contributions of both $M_J\Omega$ components to the profile is indicated. In the inset, the longitudinal phase space distribution of OH($J=3/2$, $M_J\Omega=-9/4$) radicals close to the end of the decelerator is shown, together with the separatrix, as it follows from the analytical model.

longitudinal acceptance region of the decelerator. In Fig. 1, the longitudinal emittance of the molecular beam at the entrance of the Stark decelerator is shown as the gray area, together with the overlap with the separatrices for the resonances $s=1$, 3, and 19.

When operating the decelerator at the "switching velocity" that corresponds to the mean velocity of the molecular beam $(v_{sw}=450.0$ m/s), a TOF profile as presented in Fig. 4 is observed. The main portion of the beam is transported through the machine as a compact package, and arrives in the detection region about 2.9 ms after production. The TOF profile obtained from a three-dimensional trajectory calculation, taking both $M_J\Omega$ components into account, is shown underneath the observed profile. In the simulation, no free parameters are used, except for an overall vertical scaling factor. It is assumed that directly after production both $M_J\Omega$ components are equally populated in the beam. The individual contributions of both $M_J\Omega$ components to the TOF profile is shown as well. An excellent quantitative agreement is obtained, and all features in the observed TOF profile are reproduced. The resonance mainly has contributions from the $M_J\Omega=-9/4$ component, but the individual contributions of both $M_J\Omega$ components can be identified in the wings of the distribution. The longitudinal phase-space distribution inside the decelerator can be obtained from these simulations as well, and is shown in the inset for OH radicals in the $J=3/2$, $M_J\Omega=-9/4$ state, close to the exit of the decelerator. The separatrix that follows from the model for the case $s=1$, centered around the synchronous velocity of 450 m/s, is
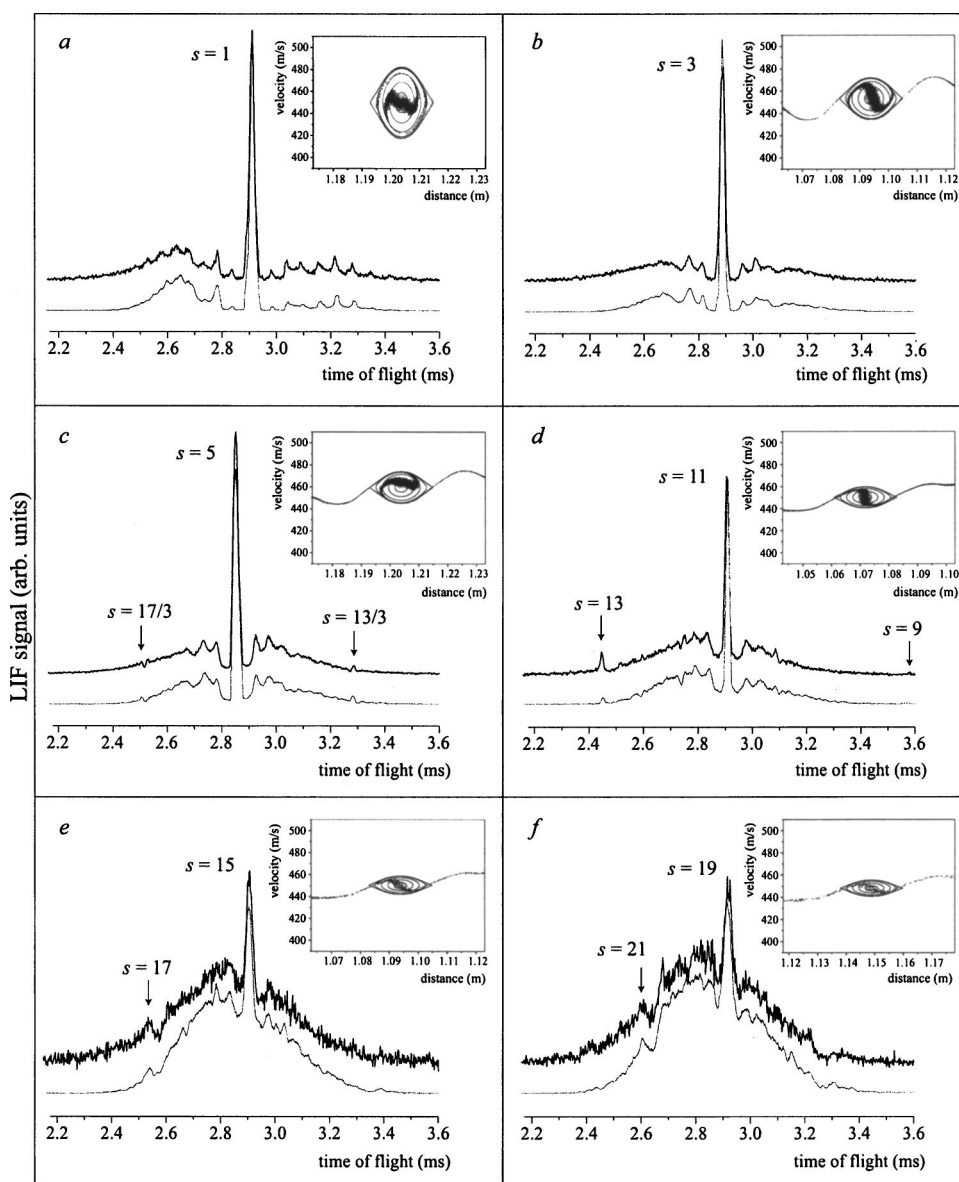
FIG. 5. Observed and simulated TOF profiles showing a series of first-order resonances with $n=1$. The decelerator is operated at phase angle $\phi_0=0°$ and a "switching velocity" $v_{sw}=$ (a) 450.0, (b) 151.1, (c) 91.9, (d) 40.9, (e) 30.0, and (f) 23.6 m/s. The TOF profiles that are obtained from three-dimensional trajectory simulations of the experiment are shown underneath the experimental profiles. In the insets, the longitudinal phase-space distributions for OH radicals in the $J=3/2$, $M_J\Omega=-9/4$ state, close to the end of the decelerator, are shown. In these phase-space plots the part of the beam that is responsible for the central feature in the observed TOF profiles is shown.

shown in the figure as well. The separatrix quantitatively describes the region in phase space where molecules oscillate around the synchronous molecule.

The velocities $s=\ell/n$ of the higher-order resonances are not within the velocity distribution of the molecular beam, and these resonances can only be observed by operating the decelerator with a lower value of v_{sw}. In Fig. 5 the observed TOF profile is shown for (a) $v_{sw}=450.0$ m/s (identical to Fig. 4), $v_{sw}=$ (b) 151.1, (c) 91.9, (d) 40.9, (e) 30.0, and (f) 23.6 m/s. In each panel a resonance is observed at a time of flight of around 2.9 ms, corresponding to a velocity (close) to 450 m/s, and can be assigned to $s=\ell=1, 3, 5, 11, 15,$ and 19 of the series $n=1$, respectively. The longitudinal acceptance of the decelerator for $\ell>1$ is compressed in the velocity direction by a factor $\sqrt{\ell}$ compared to the case $s=\ell=1$, and for increasing ℓ an ever smaller fraction of the beam is captured by the decelerator. In Figs. 5(c)–5(f), multiple resonances can be observed in a single TOF profile. The additional resonances $s=17/3, 13/3, 13, 17,$ and 21 can clearly be identified in the wings of the TOF profile. Three-

dimensional trajectory simulations again quantitatively reproduce the observed TOF profiles, and the resulting longitudinal phase space distributions for OH radicals in the $J=3/2$, $M_J\Omega=-9/4$ state are shown in the insets, together with the corresponding separatrices. In the measurements presented in the Figs. 5(b) and 5(c), the beam was not perfectly coupled in the center of the center of the longitudinal acceptance region, resulting in a slightly asymmetric phase space distribution.

In Fig. 6, TOF profiles are shown that contain a number of first-order resonances with $n>1$. The high-voltage circuitry of the decelerator does not allow us to switch faster than $v_{sw}=550$ m/s, limiting the resonances that can be observed to $s>1$. In Fig. 6(a) the time sequence of the decelerator is set to $v_{sw}=270.1$ m/s to observe the resonance $s=5/3(v_0=450.1$ m/s) at the center of the molecular-beam distribution. To correct for the phase shift of the separatrices for $n=3$, the first high-voltage pulse is applied to the decelerator when the synchronous molecule is at position $\theta=\pi/3$ in the first electric field stage. The peak at an arrival time of 2.9 ms
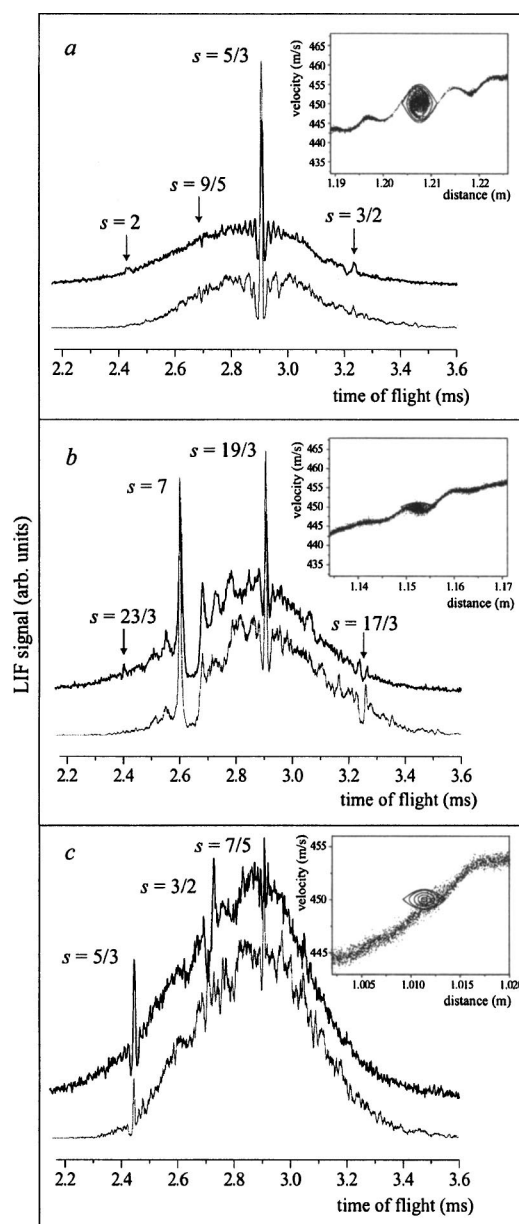
FIG. 6. Observed and simulated TOF profiles when the decelerator is operated at values of v_{sw} such that $s = \ell/n$ (ℓ and n odd; $n > 1$) resonances appear at the center of the TOF distributions. The decelerator is operated with v_{sw}= (a) 270.1, (b) 71.1, and (c) 321.5 m/s, giving rise to the resonances $s = 5/3$, $19/3$, and $7/5$ at the center of the TOF distributions, respectively.

corresponds to the resonance $s = 5/3$. The full width at half maximum of the peak is less than 10 μs, reflecting the reduced size of the corresponding separatrix compared to the series $n = 1$. Again, the three-dimensional trajectory simulation quantitatively reproduces the observed TOF profile, although the resonance $s = 5/3$ appears larger in the simulation than in the experiment. The separatrix that is obtained from the model presented in Sec. II C is shown in the inset, together with the longitudinal phase-space distribution of OH($J = 3/2, M\Omega = -9/4$) radicals near the exit of the decelerator. For reasons of clarity, the position and velocity scales are different compared to the insets of Fig. 5. In addition to

the resonance $s = 5/3$, the first-order resonance $s = 9/5$ and the second-order resonances $s = 3/2$ and 2 can be identified in the wings of the TOF distribution.

Higher resonances of the series $n = 3$ can be observed by selecting a lower value of v_{sw}, as is shown for $v_{sw} = 71.1$ m/s in Fig. 6(b). With these settings, the resonance $s = 19/3$ appears at $v_0 = 450$ m/s (arrival time around 2.9 ms). The TOF profile is dominated by the nearby resonance $s = 7$ of the (much stronger) series $n = 1$. The resonance $s = 19/3$ is again overestimated by the trajectory simulations, suggesting that the electric fields in the decelerator used in the experiment are slightly different from the calculated values. This discrepancy can be due to misalignments of the electrode array, and due to small fluctuations in the high voltage that is applied to the electrodes.

The resonances that belong to the series $n > 3$ are very weak as the coefficients a_n get increasingly smaller for higher values of n. In Fig. 6(c) the observed TOF profile is presented when the decelerator is operated with $v_{sw} = 321.5$ m/s, giving rise to the resonance $s = 7/5$ at $v_0 = 450$ m/s. The maximum extension Δv of the separatrix along the velocity axis is only 1 m/s, and the FWHM of the central peak is about 6 μs. This corresponds to a longitudinal temperature of the selected molecules of about 0.3 mK. From the inset it is seen that the beam is coupled in slightly displaced from the center of the separatrix for the resonance $s = 7/5$. The oscillation frequency ω_z is too low to observe the phase-stable rotation of the nonsynchronous molecules around the synchronous molecule in the inset. In general the TOF distribution obtained from the trajectory simulations reproduces the observed distribution well, although the resonance $s = 7/5$ appears, like the resonances $s = 5/3$ and $s = 19/3$ in Figs. 6(a) and 6(b), too large in the simulated profile. The resonance $s = 5/3$ appears too small in the simulated TOF profile. This is due to the symmetric velocity distribution of the beam that is assumed in the simulations, which results in a systematic underestimation at early arrival times of the TOF distribution. No attempt was undertaken to observe resonances with $n > 5$.

C. Second-order resonances

From the description given in Sec. II E it is clear that the size of the second-order resonances is inversely proportional to the square of the "switching velocity" v_{sw}. For realistic values of v_{sw}, these resonances are therefore expected to be equally as or less strong than the resonance $s = 7/5$. In Fig. 7, the observed and simulated TOF profiles are presented when the time sequence that is applied to the decelerator is set to observe the second-order resonances $s = 2$ [Fig. 7(a); $v_{sw} = 225.0$ m/s] and $s = 3/2$ [Fig. 7(b); $v_{sw} = 299.9$ m/s] at the center of the TOF distribution. In the observed profiles, these resonances are clearly identified at a TOF of around 2.9 ms. As expected, the resonance $s = 2$ is small, but the resonance $s = 3/2$ is surprisingly large. The agreement between the observed and simulated TOF profiles is reasonable for the resonance $s = 2$, but the size of the resonance $s = 3/2$ is not reproduced by the simulations. The longitudinal phase-space distributions that are obtained from the trajectory calcula-
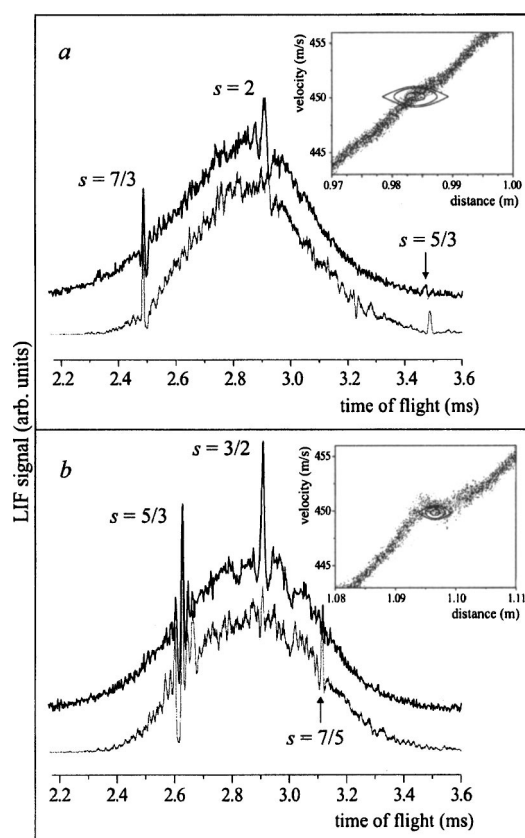
FIG. 7. Observed and simulated TOF profiles showing second-order resonances. The second-order resonances $s=2$ (a) and $3/2$ (b) are observed at the center of the TOF distribution when the decelerator is operated with a "switching velocity" of 225.0 and 299.9 m/s, respectively.

tions are shown in the insets, together with the expected separatrices from the analysis given in Sec. II E. The oscillation frequency of these resonances is too low to observe the rotation of the phase-space distribution, and only limited information on the dynamics of the molecules in the decelerator can be obtained from these figures. It is noted that the curvature around $v=450$ m/s in the phase-space distribution of Fig. 7(b) does not result from the resonance $s=3/2$, but is a remnant from the remote resonance $s=1$ (at $v=299.9$ m/s).

The disagreement between the simulations and the experiment suggests that an amplification mechanism for the resonance $s=3/2$ is present in the experiment, that is not included in the three-dimensional trajectory simulations nor in the model given in Sec. II E. Excluded in the simulated TOF profiles are, for example, the finite transient time τ of the high-voltage switches, misalignments of the electrode array, and the slight voltage drop during the burst of switch times. For the decelerator used in this work $\tau \approx 450$ ns, and simulations indicate that no effect of the transient time is to be expected on the TOF distribution. Only for τ larger than approximately 5 μs is the assumption that the fields are switched instantaneously no longer valid. Due to the finite transient time, the separatrices become somewhat smaller, and, most importantly, are phase shifted by approximately $v_{sw}\tau\pi/L$ with respect to the original separatrices. However,

this does not lead to an amplification of a resonance, and we therefore conclude that the transient time of the high-voltage switches cannot explain the discrepancy between the experiment and the trajectory simulations. Similarly, random misalignments of the electrode array and/or a voltage drop during the time sequence are only expected to result in a reduced size of the separatrices, and not in a larger resonance. The mechanical design of the decelerator is such that the distance between electrodes that are connected to the same high-voltage switch is accurately known, e.g., $2L$ is equal to 22.00 ± 0.05 mm. The mutually orthogonal arrays of electrodes might be not as exactly centered relative to each other, however, as these arrays are mounted independently. It could therefore be that the electric field stages have alternatingly a length of $(L+\Delta L)$ and $(L-\Delta L)$, where we know ΔL mechanically only up to 0.2 mm. Simulations indicate that this can only lead to a phase shift of the separatrices, but an amplification of a resonance cannot be explained. The origin of the magnitude of the resonance $s=3/2$ in the experiment, also already observed in Fig. 6(c), is therefore at present not understood.

D. Molecular beam modulation

In the previous sections, the occurrence of *phase stability* at higher velocities than the "switching velocity" v_{sw} of the decelerator has been experimentally demonstrated. In this section it is shown that these effects can also manifest themselves in the TOF profile that is observed in "normal" molecular beam deceleration experiments.

Consider a molecular beam with a mean velocity $\bar{v}$. We now apply a time sequence to the decelerator that is calculated for a synchronous molecule with initial velocity close to $\bar{v}$ and with a nonzero phase angle ϕ_0. The package of molecules that is within the corresponding separatrix ($s=1$) is decelerated from $\bar{v}$ to the final velocity, which is determined by the phase angle that is used. This process has been documented in detail in several papers [4,6], and will not be further discussed here. Instead, we will focus on the part of the beam that is not decelerated. In the time sequence, the time ΔT between successive switch times gets increasingly longer to compensate for the ever slower traveling synchronous molecule. One may wonder, therefore, if in this case phase-stable regions can be found at higher velocities than $v_{sw}=L/\Delta T$ as well. Obviously, this is not the case, as the analysis given in Secs. II B, II C, and II E shows that *simultaneous* phase stability at different values of s can only occur if the decelerator is operated at a phase angle of $0°$.[1] However, when the deceleration rate is low, the variation of ΔT is small, and the molecules moving with the resonance velocity of $sL/\Delta T$ are *almost* phase stable, i.e., the phase-space distribution of these molecules rotates around an *almost* synchronous molecule for a considerable amount of time. As the velocity of the synchronous molecule for which $s=1$ is low-

---

[1]It is noted that phase-stable deceleration of a package of molecules using a resonance with $s \neq 1$ is possible, when the appropriate time sequence is used. However, more deceleration stages compared to $s=1$ are needed to obtain the required final velocity.
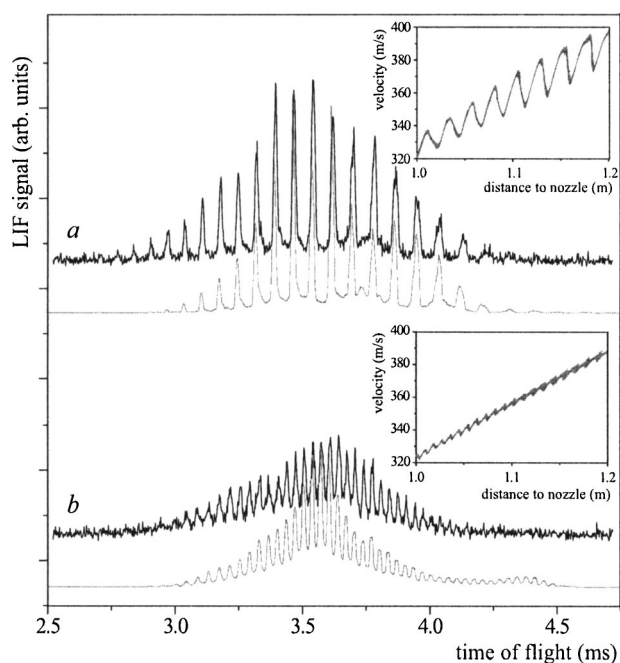
FIG. 8. Observed (upper curves) and calculated (lower curves) TOF profiles when the molecular beam is modulated by the resonance $s=$ (a) 3 and (b) 5/3. The time sequences that are applied to the decelerator have been carefully selected to obtain a maximum contrast in the TOF profile. In the insets, the phase-space distributions of OH($J=3/2$, $M_J\Omega=-9/4$) radicals are shown, when the most intense part of the beam is close to the exit of the decelerator.

ered, the velocity of a "resonance" at $s>1$ can move through the entire velocity distribution of the molecular beam, thereby inducing numerous rotations in the phase space distribution of the beam. This results in a pronounced modulation of the beam.

In Fig. 8(a), the TOF profile is shown that is observed when the molecular beam is modulated by the resonance $s=3$ that originates from the term $a_1\sin\theta$. The experiment is performed using Xe as a carrier gas, yielding a mean velocity of the beam of 365 m/s. The time sequence is selected to obtain a maximum contrast in the TOF profile. The sequence is generated for a synchronous molecule with an initial velocity of 230 m/s and for a phase angle of 40°. With these settings for the decelerator, the velocity $L/\Delta T$ of the synchronous molecule is around 100 m/s when the most intense part of the beam is close to the end of the decelerator. The velocities in the beam are well above the velocity of the synchronous molecule, and there is no part of the beam that is selected and decelerated. The velocity of the "resonance" at $s=3$, however, is lowered from 690 to 300 m/s, and moves through the complete velocity distribution of the molecular beam. A pronouncedly modulated TOF profile results, consisting of a series of peaks, with (almost) zero signal between the peaks. In the inset, the phase space distribution of the OH($J=3/2$, $M_J\Omega=-9/4$) radicals, close to the exit of the decelerator, is shown. With the time sequence used, the interaction of the beam with the $s=3$ resonance results in regions in phase space where the phase-space distribution is (nearly) vertical. A pulse train of spatially bunched mol-

ecules [23], trailing each other by 22 mm, develops, which results in the series of peaks in the TOF profile. The TOF profile that is obtained from a simulation of the experiment, taking both $M_J\Omega$ components into account, is shown underneath the experimental TOF profile, and is seen to be in quantitative agreement with the observations.

A similar modulation of the molecular beam can also be obtained when a resonance at other values of s is used. In particular, the beam can be modulated by the term $a_3\sin 3\theta$ when the velocity that corresponds to $(5/3)v_{sw}$ moves through the velocity distribution of the beam. This situation is depicted in Fig. 8(b). The decelerator is operated with a time sequence that is calculated using a phase angle $\phi_0=35°$ and for a synchronous molecule with an initial velocity of 290 m/s. When the beam is close to the end of the decelerator, about 3 ms after production, the synchronous molecule has a velocity of approximately 180 m/s. In this case, the velocity of the resonance $s=5/3$ is lowered from 485 m/s to 300 m/s, and the molecular beam strongly interacts with the term $a_3\sin 3\theta$. This results in a more finely structured modulation of the phase-space distribution of the beam (see inset) and the peaks in the TOF profile are closer spaced. The reduced contrast of the modulation is in part due to the smaller value of the coefficient a_3 compared to a_1. Again, the TOF profile that results from a numerical trajectory simulation (lower curve) accurately reproduces the experimental profile (upper curve).

Similarly rich oscillatory structure on the TOF profile of the nondecelerated beam has been observed in molecular-beam deceleration (and trapping) experiments before, but a clear explanation for this was lacking thus far. The oscillatory structure explicitly shown in the lower curve of Fig. 2 of Ref. [9], for instance, is caused by the resonance $s=5/3$, which has (partly) moved into the velocity distribution of the nondecelerated part of the beam. Although smaller in amplitude than the modulations presented here in Fig. 8, the earlier observed oscillations in Ref. [9] have the same physical origin.

IV. CONCLUSIONS

In this paper, an extended description of phase stability in a Stark decelerator, including higher-order terms in the analysis, is given. These higher-order terms give rise to a variety of phase-stable regions (resonances), which originate from the spatial and temporal periodicity of the electric fields in the decelerator. These resonances are experimentally observed using a molecular beam of OH($^2\Pi_{3/2}$, $J=3/2$) radicals. These additional resonances contribute significantly to a detailed understanding of the phase space dynamics of molecules in a Stark decelerator, and the observed TOF profiles explicitly demonstrate that ultimate control over the phase space distribution of the entire molecular beam can be obtained. This is also the main message of this paper, and at this point it is not clear whether or not these higher-order resonances will be of some practical use. In the following, we nevertheless would like to mention some possible applications.

The resonances presented in Figs. 5–7 are excellent velocity markers in the velocity distribution of the molecular

beam. In general, an accurate measurement of the velocity and velocity distribution of a molecular beam is difficult. Both the distance between nozzle and detector and the total time of flight of the molecules are often not accurately known. For the resonances described here, the velocity of the resonances is determined by two well-calibrated variables, namely, the length of the decelerator, and the total time of a burst sequence. The length of the decelerator used in this experiment is 1111 ± 0.2 mm and the accuracy of the burst sequence (with a typical duration of 2.5 ms) is given by the transient time τ of the high-voltage switches, which is about 450 ns. The accuracy with which we can determine the absolute velocity of selected resonances is therefore on the order of a few times 10^{-4}.

The observed resonances can be used to map out the electric field geometry of the decelerator; from the magnitudes of the resonances, the relative contributions of the terms $a_1 \sin \theta$, $a_3 \sin 3\theta$, $a_5 \sin 5\theta$, etc., to the potential energy of a molecule in the Stark decelerator, can be obtained. This thereby also provides a method to test the mechanical details of the electrode array.

In most experiments performed with a Stark decelerator to date, the decelerator is used either to guide ($\phi_0 = 0$) or to decelerate ($0 < \phi_0 < \pi/2$) a bunch of molecules. In principle, however, a Stark decelerator can also be used to accelerate ($-\pi/2 < \phi_0 < 0$) molecules. Although there are no intrinsic limitations to the final velocity (other than the speed of light), there are several technical constraints that are associated with the switching of the high voltage. In the decelerator used in this work, for instance, the minimum time ΔT between two successive switch times is about 20 μs, limiting the attainable final velocity to only 550 m/s if the distance L between adjacent stages is kept constant. Changing to a resonance with $s > 1$ allows one to accelerate the molecules further when the minimum allowed value of ΔT is reached, although more electric field stages are needed to obtain the required final velocity. This might be particularly important when molecules are manipulated using microstructured electrodes that are separated by only a few micrometers [24]. It is noted that in LINACs the use of multiple periods of the field for one acceleration step ($s > 1$) is very common [16].

[1] *Atomic and Molecular Beam Methods*, edited by G. Scoles (Oxford University Press, New York, 1988, 1992), Vols. 1 and 2.

[2] H. Stapelfeldt and T. Seidemann, Rev. Mod. Phys. **75**, 543 (2003).

[3] B. Friedrich, in *Modern Trends in Chemical Reaction Dynamics, Experiment and Theory (Part 1)*, edited by X. Yang and K. Liu (World Scientific, Singapore, 2004).

[4] H. L. Bethlem *et al.* Phys. Rev. A **65**, 053416 (2002).

[5] H. L. Bethlem and G. Meijer, Int. Rev. Phys. Chem. **22**, 73 (2003).

[6] H. L. Bethlem, G. Berden, and G. Meijer, Phys. Rev. Lett. **83**, 1558 (1999).

[7] J. R. Bochinski *et al.*, Phys. Rev. Lett. **91**, 243001 (2003).

[8] J. R. Bochinski *et al.*, Phys. Rev. A **70**, 043410 (2004).

[9] S. Y. T. van de Meerakker *et al.*, Phys. Rev. Lett. **94**, 023004 (2005).

[10] H. L. Bethlem *et al.*, Nature (London) **406**, 491 (2000).

[11] F. M. H. Crompvoets *et al.*, Nature (London) **411**, 174 (2001).

[12] H. L. Bethlem *et al.*, Phys. Rev. Lett. **88**, 133003 (2002).

[13] M. R. Tarbutt *et al.*, Phys. Rev. Lett. **92**, 173002 (2004).

[14] J. van Veldhoven *et al.*, Eur. Phys. J. D **31**, 337 (2004).

[15] J. J. Hudson *et al.*, Phys. Rev. Lett. **89**, 023003 (2002).

[16] S. Y. Lee, *Accelerator Physics* (World Scientific, Singapore, 1999).

[17] H. L. Bethlem *et al.*, Phys. Rev. Lett. **84**, 5744 (2000).

[18] G. Dong, W. Lu, and P. F. Barker, Phys. Rev. A **69**, 013409 (2004).

[19] R. Fulton, A. I. Bishop, and P. F. Barker, Phys. Rev. Lett. **93**, 243004 (2004).

[20] B. Friedrich, Eur. Phys. J. D **31**, 313 (2004).

[21] P. Andresen *et al.*, J. Chem. Phys. **95**, 5763 (1991).

[22] P. Andresen and E. W. Rothe, J. Chem. Phys. **82**, 3634 (1985).

[23] F. M. H. Crompvoets *et al.*, Phys. Rev. Lett. **89**, 093004 (2002).

[24] S. A. Schulz *et al.*, Phys. Rev. Lett. **93**, 020406 (2004).